MULTIMODAL MISMATCH RESPONSES IN MOUSE AUDITORY CORTEX

Magdalena Solyga[1] & Georg B. Keller[1,2]

[1]*Friedrich Miescher Institute for Biomedical Research, Basel, Switzerland.*
[2]*Faculty of Science, University of Basel, Basel, Switzerland.*

SUMMARY

Primary sensory areas of cortex have been shown to compute sensorimotor prediction errors. However, for most coupling of movement with sensory feedback, this coupling is not limited to just one sensory modality. How prediction errors in one modality influence the computation of prediction errors in another modality is still unclear. Here we use coupling between running and both auditory and visual feedback generated in a virtual environment to investigate multimodal integration of prediction errors in auditory cortex (ACx). We used two photon recordings in L2/3 of ACx to characterize responses to sounds, visual stimuli, and running onsets and found that these signals converge on a subset of L2/3 neurons. Probing responses evoked by audiomotor mismatches, we found that they closely resemble visuomotor mismatches reported previously in visual cortex (V1). Finally, testing for cross modal influence on audiomotor mismatch responses by coupling both sound amplitude and visual flow speed to the speed of running, we found that audiomotor mismatch responses were amplified when paired with concurrent audiovisual mismatches. Our results demonstrate that cross-modal and non-hierarchical interactions shape prediction error responses in cortical L2/3.

**** Dear reader, please note this manuscript is formatted in a standard submission format, and all statistical information is provided in Table S1. ****

INTRODUCTION

Prediction error like responses have been described in a variety of different cortical areas (Audette and Schneider, 2023; Ayaz et al., 2019; Han and Helmchen, 2023; Heindorf et al., 2018; Keller et al., 2012; Liu and Kanold, 2022) and across different species (Eliades and Wang, 2008; Keller and Hahnloser, 2009; Stanley and Miall, 2007). These responses are thought to be learned with experience (Attinger et al., 2017) and likely depend on local plasticity in cortex (Widmer et al., 2022). Prediction errors signal the unanticipated appearance or absence of a sensory input, and are thought to be computed as a deviation between top-down predictions and bottom-up input arriving from the sensory periphery (Rao and Ballard,

1999). One type of top-down signals that conveys a prediction of sensory input are motor-related signals. In auditory cortex, motor-related signals can modulate responses to self-generated vocalizations (Eliades and Wang, 2008) or to sounds coupled to locomotion (Schneider et al., 2018). Auditory cortex is thought to use these motor-related signals to compute audiomotor prediction error responses (Audette et al., 2022; Audette and Schneider, 2023; Eliades and Wang, 2008; Keller and Hahnloser, 2009; Liu and Kanold, 2022). These audiomotor prediction errors can be described in a hierarchical variant of predictive processing, where top-down motor-related signals function as predictions of bottom-up sensory input. While local parts of both auditory and visual processing streams are well described by a hierarchy, the cortical network as a whole does not easily map onto a hierarchical architecture, anatomically (Markov et al., 2013) or functionally (St-Yves et al., 2023; Suzuki et al., 2023) in a non-trivial way. One of the connections that does not neatly fit into a hierarchical model is the surprisingly strong connection between ACx and V1 (Clavagnier et al., 2004; Falchier et al., 2002; Ibrahim et al., 2016; Leinweber et al., 2017; Zhao et al., 2022). From ACx to V1 this connection conveys a prediction of visual input given sound (Garner and Keller, 2022), what the connection from V1 to ACx conveys, is still unclear. We argued that this connection might be a good starting point to investigate non-hierarchical interactions involved in the computation of prediction errors, and how cross-modal interactions shape sensorimotor prediction errors.

Based on this idea, we designed an experiment in which we could couple and transiently decouple running speed in a virtual environment to both self-generated auditory feedback and self-generated visual flow feedback. While doing this, we recorded activity in L2/3 neurons of ACx using two-photon calcium imaging. Using this approach, we first confirmed that a substantial subset of L2/3 neurons in ACx respond to auditory, visual and motor-related inputs. We then found that L2/3 in ACx respond to audiomotor mismatches in a way that closely resembles visuomotor mismatch responses found in V1 (Keller et al., 2012). We found no evidence of responses to visuomotor mismatch in ACx. However, when coupling both visual-flow feedback and auditory feedback to running, we found that L2/3 neurons in ACx combine information about visuomotor mismatches and audiomotor mismatches in a non-linear way. Thus, our results demonstrate that prediction errors can be potentiated by cross-modal predictions in primary sensory cortices.

57 **RESULTS**

58 **Auditory, visual, and motor signals were intermixed in L2/3 of ACx.**

59 To investigate auditory, visual, and motor signals in mouse primary auditory cortex (ACx), we combined
60 an audio-visual virtual reality system with two-photon calcium imaging in L2/3 ACx neurons (**Figure 1A**).
61 We used an adeno-associated viral (AAV) vector to express a genetically encoded calcium indicator
62 (AAV2/1-EF1α-GCaMP6f) in ACx (**Figures 1B-D**). Following 9 to 10 days of recovery after implantation
63 surgery, mice were habituated to the virtual reality setup for 5 to 7 days. We then first mapped the precise
64 location of A1 or AAF using wide-field calcium imaging (**Figure 1E**). Based on these maps, we then chose
65 recording locations for two-photon imaging of L2/3 neurons in either A1 or AAF. For the purposes of this
66 work, we did not distinguish between the two and will refer to these two areas here as ACx. During two-
67 photon imaging experiments, we recorded neuronal responses to pure tones, full-field moving gratings
68 and running onsets in ACx. We first assessed population responses of L2/3 neurons evoked by sounds
69 (pure tones presented at 4, 8, 16, or 32 kHz at either 60 dB or 75 dB SPL; **Figure 1F**). While these pure
70 tones resulted in both increases and decreases in calcium activity across the population of L2/3 neurons
71 (**Figure 1G**), the average population response across neurons exhibited a strong decrease in activity upon
72 auditory stimulation (**Figure 1H**). Next, we analyzed visual responses evoked by full-field drifting gratings
73 (8 directions; **Figure 1I**). Visual stimulation again resulted in a diverse response across the population of
74 L2/3 neurons (**Figure 1J**) but exhibited an average population response that was initially positive (**Figure**
75 **1K**). To quantify motor-related inputs to these L2/3 neurons, we then analyzed activity during running
76 onsets (**Figure 1L**). We found that the majority of neurons exhibited increases of activity during running
77 onsets (**Figure 1M**), which was also reflected in a significant positive response on the population level
78 (**Figure 1N**). Finally, we investigated how running modulates auditory and visual responses in ACx. In V1,
79 running strongly increases responses to visual stimuli (Niell and Stryker, 2010), while in auditory cortex
80 running has been shown to decrease auditory responses (Schneider et al., 2014). Separating auditory
81 responses by running state, we found that sound evoked responses of ACx neurons were similar during
82 sitting and running, but exhibited a reduced decrease in activity when the mouse was sitting (**Figure S1A**).
83 By contrast, responses to visual stimulation were enhanced during running (**Figure S1B**), similar to visual
84 responses in V1. Thus, running differentially modulates auditory and visual responses in ACx.

L2/3 neurons in ACx responded to audiomotor mismatch.

To test whether auditory, visual, and motor signals are integrated in L2/3 neurons of ACx to compute prediction errors, we first probed for responses to audiomotor (AM) mismatches. A mismatch stimulus, in this context, is the absence of a sensory input the brain predicts to receive from the environment. Thus, a mismatch is one particular type of negative prediction error. We experimentally generated a coupling between movement and sensory feedback and then used movement as a proxy for what the mouse predicts to receive as sensory feedback. To do this with an auditory stimulus, we closed-loop coupled the sound amplitude of an 8 kHz pure tone to the running speed of mouse on the spherical treadmill (**Figures 2A and 2B**). With a running speed of zero corresponding to a sound amplitude of zero, and 30 cm/s running speed corresponding to a sound amplitude of 60 dB SPL. We then introduced audiomotor mismatches by setting the sound amplitude to zero for 1 s at random times (on average every 15 s). An alternative approach to introduce audiomotor mismatches would have been to clamp the sound amplitude at a constant value. However, based on the analogy with visual flow speed in visuomotor (VM) mismatch paradigms, we chose the former. We introduce VM mismatches, by setting the visual flow speed, which is normally coupled to running speed, to zero for 1 s (Keller et al., 2012). We found that AM mismatch resulted in a strong population response (**Figure 2C and 2D**). Interestingly, this response was already apparent in the first session of coupling mice ever experienced (**Figure S2A**). To test whether AM mismatch responses can be explained simply as a sound offset response, we also performed recordings in open-loop sessions, in which we presented mice with a replay of the sound profile the mouse had self-generated in the preceding closed-loop session, including the sound playback halts. Mice were free to run during this session and did so at similar levels as during the closed-loop session (**Figure S2B**). The responses to playback halt during the open-loop session were significantly less strong than the responses to AM mismatches, independent of whether mice were running or stationary during the playback halt (**Figure 2D and S2C**). Thus, L2/3 neurons in ACx respond to AM mismatch in a way similar to the responses of L2/3 neurons in V1 to visuomotor (VM) mismatch.

Assuming that AM mismatch responses are computed as a difference between an excitatory motor-related prediction and an auditory driven inhibition, we would expect the neurons with high AM mismatch responses to exhibit opposing influence of motor and auditory input. To test this, we selected 5% of neurons with the strongest responses to AM mismatch and quantified the responses of these neurons to sound stimuli and running onsets. Consistent with a model of a subtractive computation of prediction

115 errors, we found that AM mismatch neurons exhibited a strong reduction in activity to sound stimulation
116 and an increase in activity on running onsets (**Figure 2E**). Given that mismatch responses are likely
117 enriched in the superficial part of L2/3 (O'Toole et al., 2023), and that in our two-photon imaging we also
118 preferentially record from more superficial neurons, we suspect that our population is enriched for
119 mismatch neurons. Consistent with this interpretation is the fact that we find a strong population
120 response to AM mismatches (**Figures 2C and 2D**) and a decrease in population activity to sound
121 stimulation (**Figure 1H**). Nevertheless, sound responses were significantly more negative in strong AM
122 mismatch responsive neurons than for the remainder of the population of neurons (**Figure 2F**). This effect
123 was similar when we used different thresholds for selection of audiomotor mismatch neurons (10% or
124 20% of neurons with the strongest response to AM mismatch; **Figure S3**). Also consistent with a sound
125 driven reduction of activity and running related increase of activity in AM mismatch responsive neurons,
126 we found that the correlation of calcium activity of AM mismatch neurons was negative with sound
127 amplitude and positive with running speed in open-loop sessions (**Figure 2G**). This again resembles the
128 properties of VM mismatch responses in V1 (Attinger et al., 2017). It is important to note that the sound
129 driven reduction of activity could either be the consequence of a sound driven inhibition, or a sound driven
130 reduction of excitatory input. Our data do not allow us to distinguish between these two possibilities
131 conclusively. However, assuming AM mismatch responsive neurons receive sound driven inhibition, we
132 should find that AM mismatch responsive neurons also exhibit sound playback halt responses. We would
133 expect a relief from sound driven inhibition to trigger an increase in activity assuming non-zero baseline
134 activity, while a sound driven reduction in excitation would not directly explain sound offset responses.
135 When comparing AM mismatch responses with playback halt responses for all neurons, we do indeed find
136 a positive correlation between the two (**Figure 2H**) consistent with a sound driven inhibition. Overall,
137 these results suggest that the implementation of sensorimotor prediction error computation generalizes
138 beyond V1 to other primary cortices and might be a canonical cortical mechanism.

139 **Visuomotor mismatches did not drive a population response in ACx.**

140 Visuomotor mismatch responses are likely calculated in V1 (Jordan and Keller, 2020), and spread across
141 dorsal cortex from there (Heindorf and Keller, 2023). To investigate multimodal mismatch responses, we
142 first quantified VM mismatch responses, which are independent of auditory input, in ACx. In these
143 experiments, the running speed of the mouse was coupled to the visual flow speed of the movement in a
144 virtual corridor (**Figures 3A and 3B**). We introduced VM mismatches by halting visual flow for 1 s during

145 running, as previously described (Keller et al., 2012; Zmarz and Keller, 2016). To control for visual
146 responses independent of visuomotor coupling, we again used an open-loop replay of the visual flow (see
147 Methods). We found that neither VM mismatches nor visual flow playback halts, the mouse experienced
148 in open-loop sessions, resulted in a measurable response on the population level (**Figure 3C, D**). Selecting
149 the 5% of neurons with the strongest responses to VM mismatches and quantifying their response to
150 grating presentation and running onsets, we found these neurons exhibited positive responses to running
151 onset and no significant response to grating stimulation (**Figure 3E**). These responses were not different
152 from the population responses of the remainder of the neurons (**Figure 3F**). Quantifying the correlation
153 of calcium activity with visual flow speed and running speed in the open-loop session, we found VM
154 mismatch responsive neurons to exhibit a distribution no different from chance (**Figure 3G**). This is
155 consistent with the assumption that VM mismatch responses are not computed in ACx but are inherited
156 from V1. We also found no evidence of a correlation between VM mismatch responses and playback halt
157 responses on a population level (**Figure 3H**). Thus, we conclude that while there may be a small subset of
158 VM mismatch responsive neurons in ACx, VM mismatch responses are likely relatively weak on the
159 population level and we find no evidence of a VM mismatch computation in ACx.

160 **Mismatch responses were potentiated by cross-modal interactions.**

161 Finally, we explored how multimodal coupling of both auditory and visual feedback to running speed
162 influenced mismatch responses in L2/3 of ACx. To do this, we coupled both sound amplitude and visual
163 flow speed to the running speed of the mouse in an audiovisual virtual environment (**Figures 4A and 4B**).
164 We then introduced mismatch events by halting both sound and visual flow for 1 s to trigger a concurrent
165 audiomotor and visuomotor [AM + VM] mismatch (**Figure 4B**). The nomenclature here is such that the
166 first letter in the pair denotes the sensory input that is being predicted, while the second letter denotes
167 the putative predictor – the square brackets are used to denote that the two events happen concurrently.
168 Thus, in the case of a [AM + VM] mismatch both the halted visual flow and the halted sound amplitude
169 are predicted by running speed. Please note, by "putative predictor" we mean an information source
170 available to the mouse that would in principle allow it to predict another input, given the current
171 experimental environment. The [AM + VM] mismatch resulted in a significant response on the population
172 level (**Figure 4C**). The concurrent experience of mismatch between multiple modalities could simply result
173 in a linear combination of the different mismatch signals or could result in a supra-linear combination. To
174 test whether we find evidence of a supra-linear combination of mismatch responses, we compared the

175 [AM+VM] mismatch to [AM] or an [VM] experienced in isolation. We found the presentation of a
176 [AM+VM] mismatch led to a significantly bigger response than either an [AM] or a [VM] mismatch in
177 isolation (**Figure 4D**). To test whether the linear summation of [AM] + [VM] mismatch responses could
178 explain the response to the concurrent presentation [AM+VM], we compared the two directly, and found
179 that the concurrent presentation [AM+VM] elicited a significantly larger response than the linear sum of
180 [AM] + [VM] mismatch responses (**Figure 4E**). Plotting the responses for the [AM+VM] mismatch
181 responses against the linear sum of the [AM] + [VM] mismatch responses for each neuron, we found that
182 while there is some correlation between the two, there is a subset of neurons (13.7%; blue dots, **Figure**
183 **4F**) that selectively respond to the concurrent [AM+VM] mismatch, while a different subset of neurons
184 (11.2%; purple dots, **Figure 4F**) selectively responds to the mismatch responses in isolation. This
185 demonstrates that mismatch responses in different modalities can interact non-linearly.

186 **DISCUSSION**

187 Consistent with previous reports we found that auditory, visual, and motor-related signals are intermixed
188 in the population of L2/3 neurons in ACx. Both motor-related (McGinley et al., 2015; Schneider et al.,
189 2014; Vivaldo et al., 2023; Yavorska and Wehr, 2021; Zhou et al., 2014) and visual signals (Bigelow et al.,
190 2022; Morrill and Hasenstaub, 2018; Sharma et al., 2021) have been reported across layers in ACx, with
191 the strongest running modulation found in L2/3 (Schneider et al., 2014). Also consistent with previous
192 reports we found that a subset of L2/3 neurons in ACx respond to audiomotor prediction errors (Audette
193 et al., 2022; Liu and Kanold, 2022). In V1, it has been demonstrated that neurons signaling prediction
194 errors exhibit opposing influence of bottom-up visual and top-down motor-related inputs. This has been
195 speculated to be the consequence of a subtractive computation of prediction errors (Jordan and Keller,
196 2020; Keller et al., 2012; Leinweber et al., 2017). Our findings now reveal a similar pattern of opposing
197 influence in prediction error neurons in the primary ACx that exhibit a positive correlation with motor-
198 related input and a negative correlation with auditory input (**Figure 2G**). This would be consistent with
199 the idea that both visuomotor and audiomotor prediction errors are computed as a subtraction of bottom-
200 up and top-down inputs. Based on this, it is conceivable that this type of computation extends also beyond
201 primary sensory areas of cortex and may be a more general computational principle used by cortex.

202 Finally, we found that concurrent prediction errors in multiple modalities result in an increase in
203 prediction error response that likely exceeds a linear combination of the prediction error responses in

204 single modalities (**Figure 4D**), with a subset of neurons selectively responding only to the combination of
205 prediction error responses (**Figure 4F**). A similar non-linear relationship has been described between
206 auditory and visual oddball responses in both ACx and V1 (Shiramatsu et al., 2021). At this point, it should
207 be kept in mind that deviations from linearity in terms of spiking responses are difficult to assess using
208 calcium imaging data. However, given that the difference between the concurrent presentation and the
209 linear sum of the two individual mismatch responses is approximately a factor of two (**Figure 4E**), and the
210 fact that there is a population of neurons that responds selectively to the concurrent presentation of both
211 mismatches, we suspect that also the underlying spiking responses are non-linear. What are the
212 mechanisms that could underlie this interaction? Neurons in ACx have access to information about VM
213 mismatches from at least two sources. In wide-field calcium imaging, VM mismatch responses are visible
214 across most of dorsal cortex (Heindorf and Keller, 2023). Given that we find no evidence of calcium
215 responses in L2/3 neurons (**Figure 3**), VM mismatch responses could be present in long-range cortico-
216 cortical axons, or possibly in L4, L5, or L6 neurons in ACx. An alternative source of VM mismatch input are
217 noradrenergic signals. Locus coeruleus broadcasts VM mismatch responses across the dorsal cortex
218 (Jordan and Keller, 2023). Given that the [AM+VM] mismatch responses do not simply appear to be an
219 amplified variant of the [AM] mismatch responses (**Figure 4F**), we speculate that [AM+VM] mismatch
220 responses are the result of both neuromodulatory gating and long-range cortico-cortical input from V1
221 that interact with a local computation of [AM] mismatch responses in the L2/3 ACx circuit.

222 In summary, our results demonstrate that mismatch responses in different modalities interact non-
223 linearly and can potentiate each other. What the circuit mechanisms are that underlie this form of cross-
224 modal integration of mismatch responses is still unclear and will require further investigation. However,
225 we would argue that the relatively strong cross-modal interaction demonstrates that unimodal and
226 hierarchical variants of predictive processing are insufficient to explain cortical mismatch responses. Thus,
227 if predictive processing aims to be a theory of cortical function, we will need to explore non-hierarchical
228 variants of it.

229

FIGURES

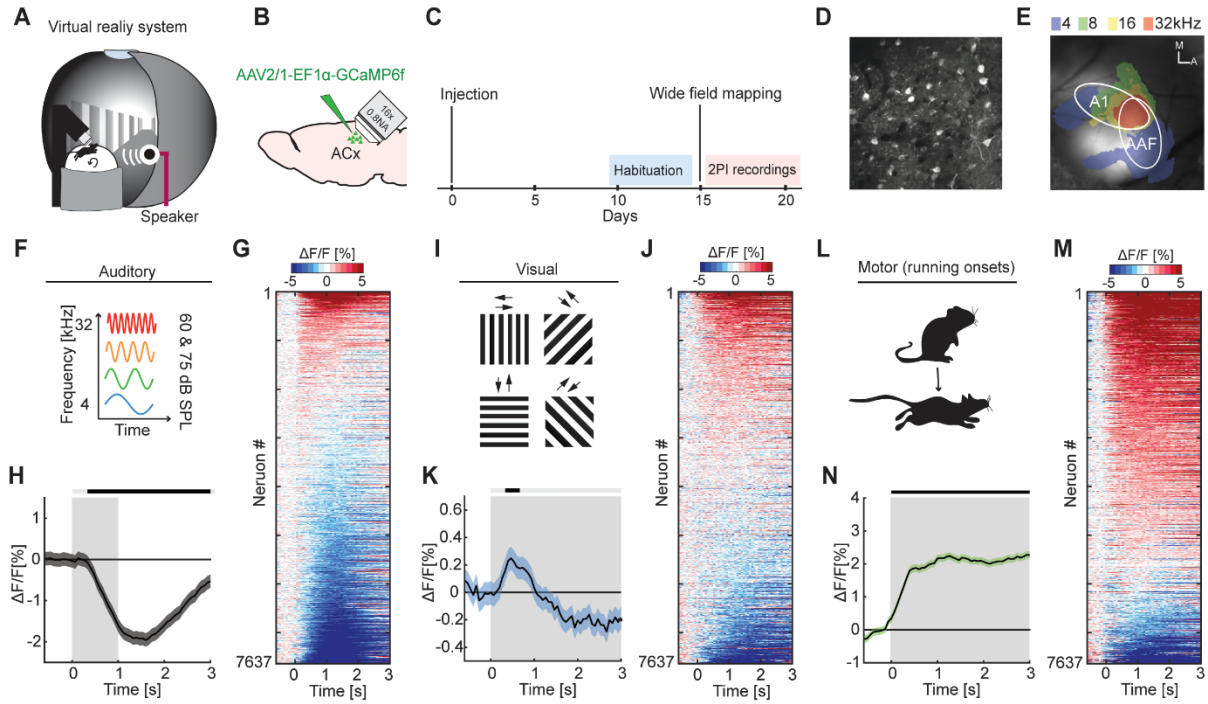

Figure 1. Auditory, visual, and motor signals were intermixed in L2/3 of ACx.

(**A**) Schematic of the virtual reality system. For imaging experiments, mice were head-fixed on an air-supported spherical treadmill. For all recordings, the scope was tilted at 45° to the left to image left ACx.

(**B**) Strategy for two-photon imaging of the ACx neurons. We injected an AAV vector expressing a genetically encoded calcium indicator in ACx.

(**C**) Timeline of the experiment. Mice were habituated to the setup without visual or auditory stimulation for 5 days starting 10 days after implantation surgery. In 1 to 6 recording sessions, one per day, we recorded data from 7637 neurons in 17 mice.

(**D**) Example two-photon image in L2/3 of the auditory cortex.

(**E**) Example wide-field mapping of the auditory cortex. Response maps reflect regions with the strongest response for each tested frequency.

(**F**) The sound stimuli we used were 1 s long pure tones of 4, 8, 16, and 32 kHz played at 60 and 75 dB SPL, presented with randomized inter trial intervals.

(**G**) The sound evoked response of all L2/3 ACx neurons sorted by response amplitude. Sound is presented from 0 s to 1 s. Red indicates an increase in activity, blue indicates a decrease in activity. All responses are baseline subtracted.

(**H**) The average population response of all L2/3 neurons to sound onset (7637 neurons). The horizontal bar above the plot marks time bins in which the response is statistically different from zero (gray: n.s., black: $p<0.05$; see Methods).

(**I**) The visual stimuli we used were full field drifting gratings of 8 different directions, presented for 4 to 8 s with randomized inter trial intervals.

(**J**) As in **G**, but for the visual responses.

(**K**) As in **H**, but for the average population response to gratings onsets (7637 neurons).

(**L**) Motor activity was assessed based on responses upon running onsets.

(**M**) As in **G**, but for running onset responses.

(**N**) As in **H**, but for the average population response to running onsets (7637 neurons).

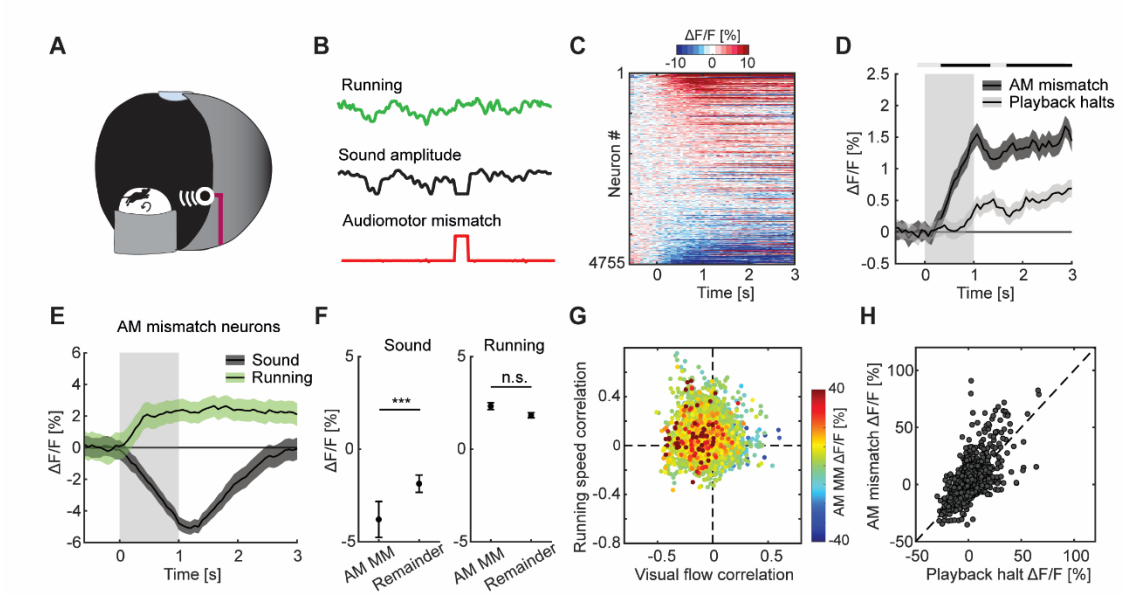

Figure 2. Primary ACx responded to audiomotor mismatch events.

(**A**) Schematic of the virtual reality system used to study responses to audiomotor mismatches. The sound amplitude of an 8 kHz pure tone was coupled to the rotation of the spherical treadmill. These experiments were performed in the darkness.

(**B**) In closed-loop sessions, the running speed of the mouse was coupled to the sound amplitude. Audiomotor mismatches were introduced by briefly setting the sound amplitude to 0 for 1 s.

(**C**) Responses of all L2/3 ACx neurons to audiomotor mismatches sorted by response amplitude.

(**D**) The average population response of all L2/3 neurons to audiomotor (AM) mismatches and sound playback halts (4755 neurons). The horizontal bar above the plot marks time bins in which the AM mismatch response is statistically different from the playback halt response (gray: n.s., black: $p<0.05$; see Methods).

(**E**) The average response of AM mismatch neurons (5 % strongest responders) to sound stimulation and running onsets.

(**F**) Comparison of the response strength of AM mismatch (MM) neurons to sound stimulation (left) and running onsets (right) compared to those of the remainder of the neuron population.

(**G**) Scatter plot of the correlation of calcium activity with sound amplitude (x-axis) and running speed (y-axis) in open-loop sessions for all neurons. The color-code reflects the strength of responses to AM mismatch in the coupled session. Note, AM mismatch responsive neurons are enriched in the upper left quadrant.

(**H**) Scatter plot of the response to audiomotor mismatch and sound playback halt for all neurons.

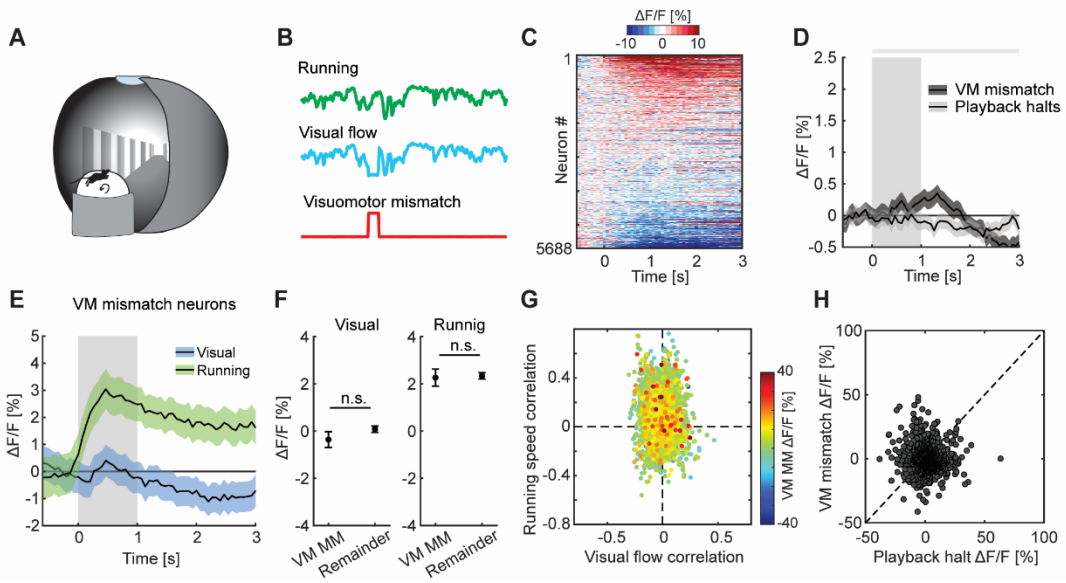

Figure 3. We found no evidence of visuomotor mismatch responses in ACx.

(**A**) Schematic of the virtual reality system used to measure visuo-motor mismatch responses. The visual flow of the virtual corridor was coupled to the rotation of the spherical treadmill. There was no sound present in these experiments.

(**B**) In closed-loop sessions, the rotation of the spherical treadmill was coupled to the movement in a virtual corridor. Visuomotor mismatches were introduced by briefly setting visual flow speed to 0 for 1 s.

(**C**) Responses of all L2/3 ACx neurons to visuomotor mismatches sorted by response amplitude.

(**D**) The average population response of all L2/3 neurons to visuomotor (VM) mismatches and visual flow playback halts (5688 neurons). The horizontal bar above the plot marks time bins in which the AM mismatch response is statistically different from the playback halt response (gray: n.s., black: $p<0.05$; see Methods).

(**E**) The average response of VM mismatch neurons (5 % strongest responders) to visual flow stimulation and running onsets.

(**F**) Comparison of the response strength of VM mismatch (MM) neurons to sound stimulation (left) and running onsets (right) compared to those of the remainder of the neuron population.

(**G**) Scatter plot of the correlation of calcium activity with visual flow speed (x-axis) and running speed (y-axis) in open-loop sessions for all neurons. The color-code reflects the strength of responses to VM mismatch in the coupled session. Note, VM mismatch responsive neurons are scattered randomly.

(**H**) Scatter plot of the response to visuomotor mismatch and visual flow playback halt for all neurons.

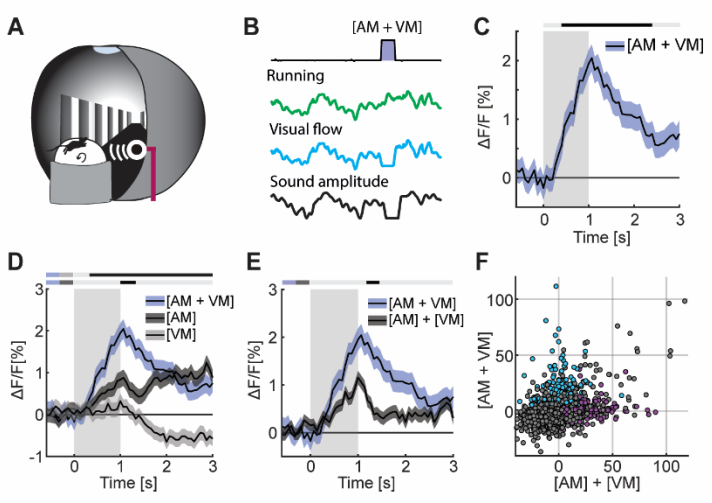

Figure 4. Mismatch responses were potentiated by cross-modal interactions in L2/3 ACx neurons.

(**A**) Schematic of the virtual reality system used to measure multimodal mismatch responses. Both the sound amplitude of 8 kHz pure tone and the movement of the visual corridor were coupled to the rotation of the spherical treadmill.

(**B**) Concurrent audiomotor and visuomotor [AM + VM] mismatches were introduced by simultaneously setting both sound amplitude and visual flow speed to 0 for 1 s.

(**C**) The average population response of all L2/3 neurons to concurrent audiomotor and visuomotor [AM + VM] mismatches (3289 neurons). The horizontal bar above the plot marks time bins in which the [AM + VM] mismatch response is statistically different from zero (gray: n.s., black: $p<0.05$; see Methods).

(**D**) Average population response of all L2/3 neurons to concurrent audiomotor and visuomotor [AM + VM] mismatches and responses evoked by the same mismatches presented separately (same data as shown in **Figures 2 and 3** but sub-selected to match the neurons that were recorded in both unimodal and multimodal mismatch paradigms; 3289 neurons). The horizontal bars above the plot mark time bins in which the [AM + VA] mismatch response is larger than the [AM] or the [VM] mismatch response (gray: n.s., black: $p<0.05$; see Methods). The two short horizontal color bars to the left of time 0 indicate which two responses are being compared.

(**E**) Average population response of all L2/3 neurons to a concurrent audiomotor and visuomotor [AM + VM] mismatches compared to the linear sum of the responses evoked by audiomotor [AM] and visuomotor [VM] mismatches presented in isolation.

(**F**) Scatter plot of the response of all neurons to the concurrent presentation of audiomotor and visuomotor [AM + VM] mismatches against the linear sum of the responses evoked by audiomotor [AM] and visuomotor [VM] mismatches presented in isolation. In blue, the subset of neurons (13.7%) that exhibited selective responses to the concurrent [AM+VM] mismatch, and in purple, the subset of neurons (11.2%) that exhibited selective responses to the linear sum of [AM] + [VM] mismatches presented in isolation. Neurons without a significant response, or that are responsive to both, are shown in gray.

SUPPLEMENTARY FIGURES

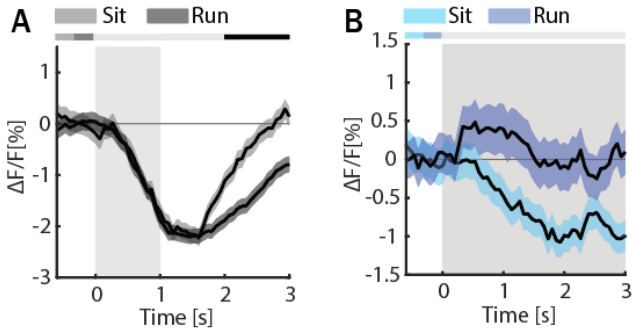

Figure S1. Effect of running on sound stimulation and moving grating responses. Related to Figure 1.

(**A**) The average population response of L2/3 neurons to sound onset (4390 neurons) during sitting (light gray) and running (dark grey). The horizontal bar above the plot marks time bins in which the response is statistically different from each other (gray: n.s., black: $p<0.05$; see Methods).

(**B**) As in **A**, but for responses to moving gratings (3701 neurons) during sitting (light blue) and running (dark blue).

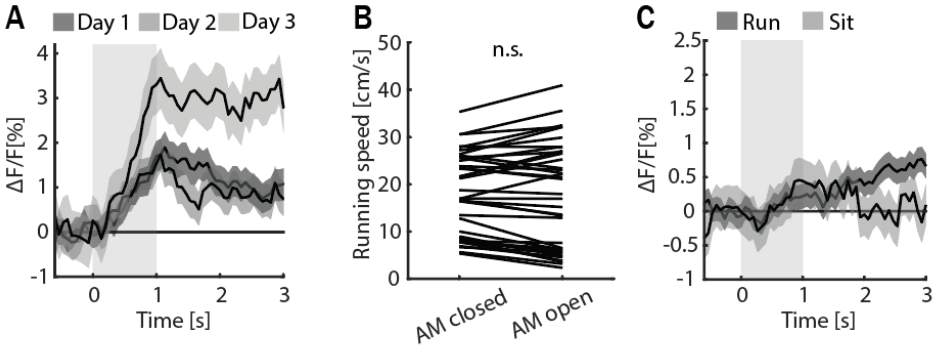

Figure S2. Controls for audiomotor mismatch responses. Related to Figure 2.

(**A**) The average population response of L2/3 neurons to audiomotor mismatches as a function of different experience with audiomotor coupling. The data shown are from the first three audiomotor closed-loop sessions. Each closed-loop session lasted 5.5 min and mice experienced one of these sessions per day (Day 1: 1271, Day 2: 904, Day 3: 453 neurons). Note, audiomotor mismatch responses are already present in the first closed-loop session.

(**B**) Comparison of running speeds during audiomotor closed and open-loop sessions.

(**C**) Comparison of the average population response of L2/3 neurons to sound playback halts while mice were running or sitting.

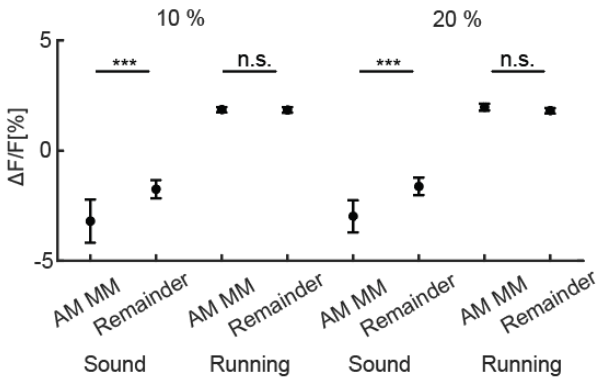

Figure S3. Related to Figure 2.

As in **Figure 2F** but using the 10% most responsive AM mismatch neurons (left), or the 20% most mismatch responsive neurons (right).

METHODS

Animals and surgery. All animal procedures were approved by and carried out in accordance with guidelines of the Veterinary Department of the Canton Basel-Stadt, Switzerland. C57BL/6 female mice (Charles River), between the ages of 7 and 12 weeks were used in this study. Mice were anesthetized using a mix of fentanyl (0.05 mg/kg), medetomidine (0.5 mg/kg), and midazolam (5 mg/kg). Analgesics were applied perioperatively. Lidocaine was injected locally on the scalp (10 mg/kg s.c.) prior to surgery, while metacam (5 mg/kg, s.c.), and buprenorphine (0.1 mg/kg s.c.) were injected just after completion of the surgery. Mice underwent a cranial window implantation surgery at an age of between 7 and 8 weeks. First, a custom-made titanium head-plate was attached to the skull (right hemisphere) with dental cement (Heraeus Kulzer). Next, a 3 mm craniotomy was made over left ACx (4.2 to 4.4 mm lateral from the midline and 2.6 to 2.8 mm posterior from bregma) followed by 4 to 6 injections of approximately 200 nl each of the AAV vector: AAV2/1-EF1α-GCaMP6f-WPRE. A circular glass cover slip was glued (Ultragel, Pattex) in place to seal the craniotomy. Mice were allowed to recover for 9 to 12 days prior to the first head fixation.

Virtual reality environment. During all recordings, mice were head-fixed in a virtual reality system, as described previously (Leinweber et al., 2014). Mice were free to run on an air-supported polystyrene ball. Three types of closed-loop conditions were used for the experiments. The rotation of the spherical treadmill was either coupled 1: to the sound amplitude (audiomotor coupling), 2: to the movement in a virtual corridor (visuomotor coupling), or 3: to both sound amplitude and the movement in a virtual corridor (audio- and visuomotor coupling). For audiomotor coupling, we used the running speed of the mouse to control the SPL of an 8 kHz tone presented to the mouse through a loudspeaker (see section auditory stimulation). This closed-loop coupling was not instantaneous but exhibited a delay of 260 ± 60 ms (mean ± STD). For visuomotor coupling, the running speed of the mouse was coupled to linear displacement in the virtual environment projected (using a Samsung SP-F10M projector synchronized to the turnaround times of the resonant scanner of the two-photon microscope) onto a toroidal screen surrounding the mouse. From the point of view of the mouse, the screen covered a visual field of approximately 240 degrees horizontally and 100 degrees vertically. The virtual environment presented on the screen was a virtual tunnel with walls consisting of continuous vertical sinusoidal gratings. Prior to the recording experiments, mice were trained in 1 to 2-hour sessions for 5 to 7 days, until they displayed regular locomotion. Closed-loop sessions were followed by an open-loop sessions, in which rotation of the spherical treadmill and sound amplitude and movement in the virtual corridor were decoupled. The

383 auditory or visual stimulus consisted of a replay of the amplitude modulated sound or visual flow recorded
384 in the previous closed-loop session.

385 **Auditory stimulation.** Sounds were generated with a 16-bit digital-to-analog converter (PCI6738, National
386 Instruments) using custom LabVIEW-based scripts (LabVIEW 2020, National Instruments) at 160 kHz
387 sampling rate, amplified (SA1, Tucker Davis Technologies, FL, USA), and played through a MF1 speaker
388 (Tucker Davis Technologies. FL, USA) positioned 10 cm from the mouse's right ear. Stimuli were calibrated
389 with a wide-band ultrasonic acoustic sensor (Model 378C01, PCB Piezotronics, NY, USA). To study sound-
390 evoked responses, we used 4, 8, 16, and 32 kHz pure tones played at 60 and 75 dB SPL (1 s duration, a
391 randomized inter-stimuli interval 4 ± 1s, ten repetitions, 1 ms on and off-ramps, randomized order). For
392 audiomotor coupling experiments, we used an 8 kHz pure tone with a sound amplitude that varied
393 between 40 and 75 dB SPL.

394 **Visual stimulation.** For visual stimulation, we used full-field drifting grating stimuli. These were composed
395 of stimuli in 8 directions (spaced by 45°) presented for a duration of 6 ± 2 s with a randomized inter-stimuli
396 interval of 4.5 ± 1.5 s (gray screen). The sequence of stimuli presented was randomized.

397 **Running onsets.** Running onsets were defined as the running speed crossing a threshold of 5 cm/s, where
398 the average speed in the previous three seconds was below 4 cm/s. To separate stimulus trials into
399 running and sitting, we used a threshold of 2.2 cm/s in a 1 s window preceding the stimulus onset.

400 **Wide-field fluorescence imaging.** To establish a reference tonotopic map of A1 and AAF, we performed
401 wide-field fluorescence imaging experiments on a custom-built microscope consisting of objectives
402 mounted face-to-face (Nikon 85 mm/f1.8 sample side, Nikon 50 mm/f1.4 sensor side), as previously
403 described (Heindorf and Keller, 2023). Blue illumination was provided by a light-emitting diode (470 nm,
404 Thorlabs) and passed through an excitation filter (SP490, Thorlabs). Green fluorescence emission was
405 filtered with a 525/50 bandpass filter. Images were acquired at a frame rate of 100 Hz on a sCMOS camera
406 (PCO edge 4.2). The raw images were cropped on-sensor, and the resulting data was streamed to disk
407 with custom-written software in LabVIEW (National Instruments).

408 **Two-photon imaging.** Calcium imaging of L2/3 neurons in A1 and AAF was performed using a modified
409 Thorlabs Bergamo II microscope with a 16x, 0.8 NA objective (Nikon N16XLWD-PF), as previously
410 described (Leinweber et al., 2014). To record in left ACx, the scope was tilted 45° to the left. The excitation
411 light source was a tunable, femtosecond-pulsed laser (Insight, Spectra Physics or Chameleon, Coherent)

412 tuned to 930 nm. The laser power was adjusted to 30 mW. A 12-kHz resonance scanner (Cambridge
413 Technology) was used for line scanning, and we acquired 400 lines per frame. This resulted in a frame rate
414 of 60 Hz at a resolution of 400 × 750 pixels. We used a piezo-electric linear actuator (Physik Instrumente,
415 P-726) to record from 4 z-layers, separated by 15 µm, in an interleaved manner. This reduced the effective
416 frame rate per layer to 15 Hz. The emission light was bandpass filtered using a 525/50 nm filter (Semrock),
417 and signals were detected with a photomultiplier (Hamamatsu, H7422), amplified (Femto, DHCPCA-100),
418 digitized at 800 MHz (National Instruments, NI5772), and bandpass filtered at 80 MHz with a digital
419 Fourier-transform filter on a field-programmable gate array (National Instruments, PXIe-7965). Recording
420 locations were visually registered against the reference images acquired with wide-field imaging
421 previously using blood vessels patterns.

422 **Wide-field image analysis.** Off-line data processing and data analysis were done with custom-written
423 MATLAB scripts. Slow drifts in the fluorescence signal were removed using 8th percentile filtering with a
424 62.5 s moving window, similar to what is used for two-photon imaging data (Dombeck et al., 2007).
425 Activity was calculated as the $\Delta F/F_0$, where F_0 was the median fluorescence over the entire recording. For
426 stimulus responses, we use a response window of 0.2 s to 1.2 s following stimulus onset and a baseline
427 window of -1 s to 0 s before stimulus onset. The pixels with the strongest response (3-5% of pixels), were
428 used to mark the tonotopic areas corresponding to the different stimuli.

429 **Two-photon image analysis.** Calcium imaging data were processed as described previously. In brief, raw
430 images were full-frame registered to correct lateral brain motion. Neurons were selected manually based
431 on mean and maximum fluorescence images. Average fluorescence per neuron over time was corrected
432 for slow fluorescence drift using an 8th percentile filter and a 100 s window (Dombeck et al., 2007; Keller
433 et al., 2012) and divided by the median value over the entire trace to calculate $\Delta F/F_0$. All stimulus-response
434 curves were baseline subtracted. The baseline subtraction window was -0.5 s to 0 s before stimulus onset.
435 For quantification of responses during all onset types (auditory, visual, running, mismatch), $\Delta F/F$ was
436 averaged over the response time window (0.5 s to 2.5 s after stimulus onset) and baseline subtracted
437 (mean activity in a window preceding stimulus onset, -0.5 s to 0 s). Triggers happening with smaller
438 intervals than 2 s, which were not preceded by at least 2 s of baseline or not followed by at least 3 s of
439 recording time, were omitted from the analysis. Sessions with less than two triggers were not included in
440 the analysis. To quantify the difference of average calcium responses as a function of time, we used a

441 hierarchical bootstrap test for every 5 frames of the calcium trace (330 ms) and marked comparisons
442 where responses were different ($p < 0.05$).

443 **Statistical tests.** All statistical information for the tests performed in this manuscript is provided in Table
444 S1. We used hierarchical bootstrapping (Saravanan et al., 2020) for statistical testing due to the nested
445 structure of the data (multiple neurons from one imaging site). We first resampled the data with
446 replacement (replications of previously drawn samples are allowed) at the level of imaging sites, followed
447 by resampling at the level of neurons. We then computed the mean responses across the resampled
448 population and repeated the process 10 000 times. The probability of one group being different from the
449 other was calculated as a fraction of bootstrap sample means which violated the tested hypothesis.

450

Table S1. Statistics

All information on statistical tests used in this manuscript are shown in Table S1 below. We used hierarchical bootstrap (Saravanan et al., 2020) or a correlation coefficient for all comparisons.

Figure	Description	Test	N_1 (mice)	N_2 (mice)	Unit	P-value
Figure 2G	Sound	Bootstrap	4755 (38 sessions, 12 mice)	4755 (38 sessions, 12 mice)	Neurons	0.0014
Figure 2G	Running	Bootstrap	4755 (38 sessions, 12 mice)	4755 (38 sessions, 12 mice)	Neurons	0.27
Figure 2H	AM closed vs AM open	Correlation	4755 (38 sessions, 12 mice)	4755 (38 sessions, 12 mice)	Neurons	$p < 0.001$ $r = 0.66$
Figure 3G	Visual	Bootstrap	5688 (47 sessions, 15 mice)	5688 (47 sessions, 15 mice)	Neurons	0.31
Figure 3G	Running	Bootstrap	5688 (47 sessions, 15 mice)	5688 (47 sessions, 15 mice)	Neurons	0.61
Figure 3H	VM closed vs VM open	Correlation	5688 (47 sessions, 15 mice)	5688 (47 sessions, 15 mice)	Neurons	$p = 0.41$ $r = 0.01$
Figure 4F	[AM + VM] vs [AM] + [VM]	Correlation	3289 (26 sessions, 10 mice)	3289 (26 sessions, 10 mice)	Neurons	$p < 0.001$ $r = 0.31$
Figure S2B	AM closed vs AM open	Bootstrap	38 sessions (12 mice)	38 sessions (12 mice)	Neurons	0.47

456 **Key Resource Table**

REAGENT or RESOURCE	Source	Identifier
Bacterial and virus strains		
AAV2/1-EF1α-GCaMP6f-WPRE (10^{14} GC/ml)	FMI vector core	vector.fmi.ch
Chemicals, peptides, and recombinant proteins		
Fentanyl citrate	Actavis	CAS 990-73-8
Midazolam (Dormicum)	Roche	CAS 59467-96-8
Medetomidine (Domitor)	Orion Pharma	CAS 86347-14-0
Ropivacaine	Presenius Kabi	CAS 132112-35-7
Lidocaine	Bichsel	CAS 137-58-6
Buprenorphine	Reckitt Benckiser Healthcare	CAS 52485-79-7
Ophthalmic gel (Humigel)	Virbac	N/A
Flumazenil (Anexate)	Roche	CAS 78755-81-4
Atipamezole (Antisedan)	Orion Pharma	CAS 104054-27-5
N-Butyl-2-cyanoacrylate (Histoacryl)	Braun	CAS 6606-65-1
Dental cement (Paladur)	Heraeus Kulzer	CAS 9066-86-8
Meloxicam (Metacam)	Boehringer Ingelheim	CAS 71125-39-8
Deposited data		
All data and code used to generate manuscript figures	This paper	data.fmi.ch
Experimental models: Organisms/strains		
Mus musculus: C57BL/6	Charles River	N/A
Software and algorithms		
MATLAB (2021b)	The MathWorks	RRID: SCR_001622
LabVIEW	National Instruments	RRID: SCR_014325
Python	python.org	RRID: SCR_008394
Panda3D	panda3d.org	N/A

457

458 **ACKNOWLEDGEMENTS**

459 We thank Tingjia Lu for the production of viral vectors and all the members of the Keller lab for discussion
460 and support. This project has received funding from the Swiss National Science Foundation (GBK), the
461 Novartis Research Foundation (GBK), and the European Research Council (ERC) under the European
462 Union's Horizon 2020 research and innovation programme (grant agreement No 865617) (GBK).

463 **AUTHOR CONTRIBUTIONS**

464 MS designed and performed the experiments and analyzed the data. All authors wrote the manuscript.

465 **DECLARATION OF INTERESTS**

466 The authors declare no competing financial interests.

REFERENCES

Attinger, A., Wang, B., Keller, G.B., 2017. Visuomotor Coupling Shapes the Functional Development of Mouse Visual Cortex. Cell 169, 1291-1302.e14. https://doi.org/10.1016/j.cell.2017.05.023

Audette, N.J., Schneider, D.M., 2023. Stimulus-specific prediction error neurons in mouse auditory cortex. https://doi.org/10.1101/2023.01.06.523032

Audette, N.J., Zhou, W., La Chioma, A., Schneider, D.M., 2022. Precise movement-based predictions in the mouse auditory cortex. Curr Biol 32, 4925-4940.e6. https://doi.org/10.1016/j.cub.2022.09.064

Ayaz, A., Stäuble, A., Hamada, M., Wulf, M.A., Saleem, A.B., Helmchen, F., 2019. Layer-specific integration of locomotion and sensory information in mouse barrel cortex. Nature Communications 10, 1–14. https://doi.org/10.1038/s41467-019-10564-8

Bigelow, J., Morrill, R.J., Olsen, T., Hasenstaub, A.R., 2022. Visual modulation of firing and spectrotemporal receptive fields in mouse auditory cortex. Current Research in Neurobiology 3, 100040. https://doi.org/10.1016/j.crneur.2022.100040

Clavagnier, S., Falchier, A., Kennedy, H., 2004. Long-distance feedback projections to area V1: Implications for multisensory integration, spatial awareness, and visual consciousness. Cognitive, Affective, & Behavioral Neuroscience 4, 117–126. https://doi.org/10.3758/CABN.4.2.117

Dombeck, D.A., Khabbaz, A.N., Collman, F., Adelman, T.L., Tank, D.W., 2007. Imaging large-scale neural activity with cellular resolution in awake, mobile mice. Neuron 56, 43–57. https://doi.org/10.1016/j.neuron.2007.08.003

Eliades, S.J., Wang, X., 2008. Neural substrates of vocalization feedback monitoring in primate auditory cortex. Nature 453, 1102–6. https://doi.org/10.1038/nature06910

Falchier, A., Clavagnier, S., Barone, P., Kennedy, H., 2002. Anatomical evidence of multimodal integration in primate striate cortex. J Neurosci 22, 5749–5759. https://doi.org/10.1523/JNEUROSCI.22-13-05749.2002

Garner, A.R., Keller, G.B., 2022. A cortical circuit for audio-visual predictions. Nat Neurosci 25, 98–105. https://doi.org/10.1038/s41593-021-00974-7

Han, S., Helmchen, F., 2023. Behavior-relevant top-down cross-modal predictions in mouse neocortex. https://doi.org/10.1101/2023.04.03.535389

Heindorf, M., Arber, S., Keller, G.B., 2018. Mouse Motor Cortex Coordinates the Behavioral Response to Unpredicted Sensory Feedback. Neuron 99, 1040-1054.e5. https://doi.org/10.1016/j.neuron.2018.07.046

Heindorf, M., Keller, G.B., 2023. Antipsychotic drugs selectively decorrelate long-range interactions in deep cortical layers. https://doi.org/10.1101/2022.01.31.478462

Ibrahim, L.A., Mesik, L., Ji, X.-Y., Fang, Q., Li, H.-F., Li, Y.-T., Zingg, B., Zhang, L.I., Tao, H.W., 2016. Cross-Modality Sharpening of Visual Cortical Processing through Layer-1-Mediated Inhibition and Disinhibition. Neuron 89, 1031–1045. https://doi.org/10.1016/j.neuron.2016.01.027

Jordan, R., Keller, G.B., 2020. Opposing Influence of Top-down and Bottom-up Input on Excitatory Layer 2/3 Neurons in Mouse Primary Visual Cortex. Neuron 108, 1194-1206.e5. https://doi.org/10.1016/j.neuron.2020.09.024

Keller, G.B., Bonhoeffer, T., Hübener, M., 2012. Sensorimotor Mismatch Signals in Primary Visual Cortex of the Behaving Mouse. Neuron 74, 809–815. https://doi.org/10.1016/j.neuron.2012.03.040

Keller, G.B., Hahnloser, R.H.R., 2009. Neural processing of auditory feedback during vocal practice in a songbird. Nature 457, 187–90. https://doi.org/10.1038/nature07467

Leinweber, M., Ward, D.R., Sobczak, J.M., Attinger, A., Keller, G.B., 2017. A Sensorimotor Circuit in Mouse Cortex for Visual Flow Predictions. Neuron 95, 1420-1432.e5. https://doi.org/10.1016/j.neuron.2017.08.036

Leinweber, M., Zmarz, P., Buchmann, P., Argast, P., Hübener, M., Bonhoeffer, T., Keller, G.B., 2014. Two-photon calcium imaging in mice navigating a virtual reality environment. Journal of visualized experiments : JoVE e50885.

Liu, J., Kanold, P.O., 2022. Interactive auditory task reveals complex sensory-action integration in mouse primary auditory cortex. https://doi.org/10.1101/2022.12.12.520155

Markov, N.T., Ercsey-Ravasz, M., Van Essen, D.C., Knoblauch, K., Toroczkai, Z., Kennedy, H., 2013. Cortical high-density counterstream architectures, Science. American Association for the Advancement of Science. https://doi.org/10.1126/science.1238406

McGinley, M.J., David, S.V., McCormick, D.A., 2015. Cortical Membrane Potential Signature of Optimal States for Sensory Signal Detection. Neuron 87, 179–192. https://doi.org/10.1016/j.neuron.2015.05.038

Morrill, R.J., Hasenstaub, A.R., 2018. Visual Information Present in Infragranular Layers of Mouse Auditory Cortex. J Neurosci 38, 2854–2862. https://doi.org/10.1523/JNEUROSCI.3102-17.2018

Niell, C.M., Stryker, M.P., 2010. Modulation of visual responses by behavioral state in mouse visual cortex. Neuron 65, 472–9. https://doi.org/10.1016/j.neuron.2010.01.033

O'Toole, S.M., Oyibo, H.K., Keller, G.B., 2023. Molecularly targetable cell types in mouse visual cortex have distinguishable prediction error responses. Neuron 111, 2918-2928.e8. https://doi.org/10.1016/j.neuron.2023.08.015

Rao, R.P.N., Ballard, D.H., 1999. Predictive coding in the visual cortex: a functional interpretation of some extra-classical receptive-field effects. Nature Neuroscience 2, 79–87. https://doi.org/10.1038/4580

Rebecca, J., B, K.G., 2023. The locus coeruleus broadcasts prediction errors across the cortex to promote sensorimotor plasticity. eLife 12. https://doi.org/10.7554/eLife.85111

Saravanan, V., Berman, G.J., Sober, S.J., 2020. Application of the hierarchical bootstrap to multi-level data in neuroscience. Neuron Behav Data Anal Theory 3, https://nbdt.scholasticahq.com/article/13927-application-of-the-hierarchical-bootstrap-to-multi-level-data-in-neuroscience.

Schneider, D.M., Nelson, A., Mooney, R., 2014. A synaptic and circuit basis for corollary discharge in the auditory cortex. Nature 513, 189–194. https://doi.org/10.1038/nature13724

Schneider, D.M., Sundararajan, J., Mooney, R., 2018. A cortical filter that learns to suppress the acoustic consequences of movement. Nature 561, 391–395. https://doi.org/10.1038/s41586-018-0520-5

Sharma, S., Srivastava, H.K., Bandyopadhyay, S., 2021. Modulation of auditory responses by visual inputs in the mouse auditory cortex. https://doi.org/10.1101/2021.01.22.427870

Shiramatsu, T.I., Mori, K., Ishizu, K., Takahashi, H., 2021. Auditory, Visual, and Cross-Modal Mismatch Negativities in the Rat Auditory and Visual Cortices. Front Hum Neurosci 15, 721476. https://doi.org/10.3389/fnhum.2021.721476

Stanley, J., Miall, R.C., 2007. Functional activation in parieto-premotor and visual areas dependent on congruency between hand movement and visual stimuli during motor-visual priming. NeuroImage 34, 290–9. https://doi.org/10.1016/j.neuroimage.2006.08.043

St-Yves, G., Allen, E.J., Wu, Y., Kay, K., Naselaris, T., 2023. Brain-optimized deep neural network models of human visual areas learn non-hierarchical representations. Nat Commun 14, 3329. https://doi.org/10.1038/s41467-023-38674-4

Suzuki, M., Pennartz, C.M.A., Aru, J., 2023. How deep is the brain? The shallow brain hypothesis. Nat. Rev. Neurosci. 1–14. https://doi.org/10.1038/s41583-023-00756-z

Vivaldo, C.A., Lee, J., Shorkey, M., Keerthy, A., Rothschild, G., 2023. Auditory cortex ensembles jointly encode sound and locomotion speed to support sound perception during movement. PLOS Biology 21, e3002277. https://doi.org/10.1371/journal.pbio.3002277

Widmer, F.C., O'Toole, S.M., Keller, G.B., 2022. NMDA receptors in visual cortex are necessary for normal visuomotor integration and skill learning. eLife 11, e71476. https://doi.org/10.7554/eLife.71476

Yavorska, I., Wehr, M., 2021. Effects of Locomotion in Auditory Cortex Are Not Mediated by the VIP Network. Front Neural Circuits 15, 618881. https://doi.org/10.3389/fncir.2021.618881

Zhao, M., Ren, M., Jiang, T., Jia, X., Wang, X., Li, A., Li, X., Luo, Q., Gong, H., 2022. Whole-Brain Direct Inputs to and Axonal Projections from Excitatory and Inhibitory Neurons in the Mouse Primary Auditory Area. Neurosci Bull 38, 576–590. https://doi.org/10.1007/s12264-022-00838-5

Zhou, M., Liang, F., Xiong, X.R., Li, L., Li, H., Xiao, Z., Tao, H.W., Zhang, L.I., 2014. Scaling down of balanced excitation and inhibition by active behavioral states in auditory cortex. Nat Neurosci 17, 841–850. https://doi.org/10.1038/nn.3701

Zmarz, P., Keller, G.B., 2016. Mismatch Receptive Fields in Mouse Visual Cortex. Neuron 92, 766–772. https://doi.org/10.1016/j.neuron.2016.09.057